PERGAMON

International Journal of Heat and Mass Transfer 42 (1999) 2673–2681

International Journal of HEAT and MASS TRANSFER

Effect of anisotropy on transport phenomena in anisotropic porous media

J.H. Yang, S.L. Lee*

Department of Power Mechanical Engineering, National Tsing-Hua University, Hsinchu 30043, Taiwan

Received 12 December 1997; in final form 26 June 1998

Abstract

The effect of anisotropy on transport phenomena in anisotropic porous media is studied in this paper. For convenience, a bank of circular cylinders which can be treated as an anisotropic porous medium is employed such that both Darcy-Forchheimer drag and effective thermal conductivity can be accurately determined. Two problems including a forced flow and a natural convection are illustrated to investigate the effect of anisotropy on fluid flow and heat transfer through a bank of circular cylinders. The solutions reveal that inclination of the cylinder bundle could give rise to an influence of more than 100% on the heat transfer rate for both forced convection and natural convection. Hence, the anisotropy of an anisotropic porous medium should not be ignored.

Nomenclature

c_p specific heat [J kg^{-1} K^{-1}]
d granule size of the porous medium [m]
F Forchheimer coefficient, equation (8a)
g gravity [9.806 m s^{-2}]
Gr_c characteristic Grashof number, $\beta g \Delta T L/V_c^2$
H width of a channel or a square enclosure [m]
K permeability of a porous medium [m^2]
k thermal conductivity [W m^{-1} K^{-1}]
L characteristic length [m]
l row spacing of the cylinder bank [m]
$\dot{m}$ mass flow rate [kg s^{-1}]
$\bar{P}$ pressure on the superficial flow [N m^{-2}]
$\bar{p}$ dimensionless pressure, $\bar{P}/(\rho_f V_c^2)$
Pe_c characteristic Peclet number, $V_c L/\alpha_f$
Pr Prandtl number, v/α_f
Q heat transfer from the heating plate [W m^{-1}]
q dimensionless heat transfer rate, equations (24) and (30)
R_{xx}, R_{xy}, R_{yx}, R_{yy} dimensionless tensor of Darcy–Forchheimer drag
Ra Rayleigh number, $\beta g \Delta T H^3/\alpha_f v$
Re Reynolds number, $U_m H/v$
Re_c characteristic Reynolds number, $V_c L/v$
$(Re_d)_{11}$ granule Reynolds number, $|\bar{U}_{11}|d/v$
T temperature [K]
T_o, T_∞ some constant temperatures [K]
$(\bar{U}, \bar{V})$ superficial velocity [m s^{-1}]
$(\bar{u}, \bar{v})$ dimensionless superficial velocity
$\bar{U}_m$ mean velocity, $\dot{m}/(\rho_f H)$
V_c characteristic velocity [m s^{-1}]
W heating length in the forced convection case [m]
(X, Y) coordinate system [m]
(x, y) dimensionless coordinates, $(X/L, Y/L)$.

Greek symbols
α thermal diffusivity [m^2 s^{-1}]
β volumetric thermal expansion [K^{-1}]
ΔT characteristic temperature [K]
ε porosity
θ dimensionless temperature, $(T-T_\infty)/\Delta T$
κ dimensionless thermal conductivity, k/k_f
κ_{xx}, κ_{xy}, κ_{yx}, κ_{yy} tensor of effective thermal conductivity
μ dynamic viscosity [N s m^{-2}]
v kinematic viscosity [m^2 s^{-1}], μ/ρ
ρ density [kg m^{-3}]
σ thermal conductivity ratio, k_s/k_f
ϕ inclination angle of the cylinders [deg]
ψ stream function, equation (29).

Subscripts
11, 22, 33 tensor indexes in principal coordinates
c characteristic

* Corresponding author.

0017–9310/99/$ - see front matter
PII: S0017–9310(98)00334–2

f fluid
max maximum
min minimum
ref reference
s solid.

1. Introduction

Fluid flow and heat transfer through anisotropic porous media find many applications in industry and in nature. However, the permeability of porous media depends very strongly on its microstructure [1]. This leads to a great difficulty in the determination of the Darcy–Forchheimer drag for random heterogeneous porous media, especially when they are macroscopically anisotropic. Thus, the literature dealing with the anisotropic effect in anisotropic porous media are very limited.

In his study, Poirier [2] modelled a bank of circular cylinders as an anisotropic porous medium. A correlation from the available experimental data was obtained for the principal permeabilities (K_{11} and K_{22}) that were parallel and normal to the cylinders. However, Poirier's correlation was restricted to a porosity of the range $0.19 \leqslant \varepsilon \leqslant 0.66$, while the error of the correlation could be as large as 43%. Based on a simplified form of Poirier's correlation, Sinha et al. [3] found that the anisotropic effect of the dendrites was significant in alloy solidification if the extent of the mushy zone was large or if the Rayleigh number was high. To investigate the anisotropic effect, Yoo and Viskanta [4] assumed the principal permeability K_{11} was of the Blake–Kozeny type. However, a value was assigned to the permeability ratio (K_{22}/K_{11}) due to the lack of appropriate information. The influence of the anisotropy on the transport phenomena thus was not properly observed.

Many attempts were also undertaken to improve the upper and lower bounds for the permeability of some particular porous media [1]. Logically, porous media of the same porosity could have entirely different permeability. For instance, for a flow across a bank of circular cylinders that can be treated as a porous medium, it is possible to achieve a zero permeability in one direction (say X) at a given porosity ε by letting the clearance of the cylinders be zero in the other direction (say Y). Narrow bound widths thus are not expected for most microstructures discussed in the review [1]. As a result, the estimated bounds could be too divergent to have utility in practical applications.

It should be pointed out here that many porous media possess a definite and regular microstructure especially for that from industry. Fluid flow and heat transfer through a cylinder (tube) bundle is one of the examples. The purpose of the present study is to investigate the effect of the anisotropy on fluid flow and heat transfer through an anisotropic porous medium. For simplicity, a bank of circular cylinders is employed such that both principal permeability and effective thermal conductivity can be accurately determined. Two examples including a forced flow and a natural convection will be conducted to study the anisotropic effect on the transport phenomena.

2. Theoretical analysis

Consider a fluid flow and heat transfer through an anisotropic porous medium of homogeneous porosity ε. All of the thermophysical properties are constant. The flow is assumed steady, laminar, incompressible and macroscopically two-dimensional. The solid phase has reached thermal equilibrium with the fluid phase. The coordinates are properly arranged such that the gravity is in the $-y$ direction. After introducing the Boussinesq approximation and the dimensionless transformation

$$\bar{u} = \bar{U}/V_c, \quad \bar{v} = \bar{V}/V_c, \quad x = X/L, \quad y = Y/L,$$
$$\bar{p} = \bar{P}/(\rho_f V_c^2), \quad \kappa = k/k_f, \quad \alpha_f = (k/\rho c_p)_f,$$
$$\theta = (T - T_\infty)/\Delta T, \quad Re_c = V_c L/\nu,$$
$$Gr_c = \beta g \Delta T L/V_c^2, \quad Pe_c = V_c L/\alpha_f \tag{1}$$

the governing equations become [3–8]

$$\frac{\partial \bar{u}}{\partial x} + \frac{\partial \bar{v}}{\partial y} = 0 \tag{2}$$

$$\frac{1}{\varepsilon}\left(\bar{u}\frac{\partial \bar{u}}{\partial x} + \bar{v}\frac{\partial \bar{u}}{\partial y}\right) = -\varepsilon\frac{\partial \bar{p}}{\partial x} + \frac{1}{Re_c}\left(\frac{\partial^2 \bar{u}}{\partial x^2} + \frac{\partial^2 \bar{u}}{\partial y^2}\right) - \varepsilon\frac{1}{Re_c}\left(\frac{L}{d}\right)^2 (R_{xx}\bar{u} + R_{xy}\bar{v}) \tag{3}$$

$$\frac{1}{\varepsilon}\left(\bar{u}\frac{\partial \bar{v}}{\partial x} + \bar{v}\frac{\partial \bar{v}}{\partial y}\right) = -\varepsilon\frac{\partial \bar{p}}{\partial y} + \frac{1}{Re_c}\left(\frac{\partial^2 \bar{v}}{\partial x^2} + \frac{\partial^2 \bar{v}}{\partial y^2}\right) - \varepsilon\frac{1}{Re_c}\left(\frac{L}{d}\right)^2 (R_{yx}\bar{u} + R_{yy}\bar{v}) + \varepsilon\, Gr_c(\theta - \theta_{ref}) \tag{4}$$

$$Pe_c\left(\bar{u}\frac{\partial \theta}{\partial x} + \bar{v}\frac{\partial \theta}{\partial y}\right) = \frac{\partial}{\partial x}\left(\kappa_{xx}\frac{\partial \theta}{\partial x}\right) + \frac{\partial}{\partial x}\left(\kappa_{xy}\frac{\partial \theta}{\partial y}\right) + \frac{\partial}{\partial y}\left(\kappa_{yx}\frac{\partial \theta}{\partial x}\right) + \frac{\partial}{\partial y}\left(\kappa_{yy}\frac{\partial \theta}{\partial y}\right) \tag{5}$$

where V_c, L and ΔT are respectively the characteristic velocity, the characteristic length and the characteristic temperature, while T_∞ denotes a temperature level. The notation $(\bar{U}, \bar{V})$ denotes the superficial velocity. The granule size of the porous medium d/L, the characteristic Reynolds number Re_c, the characteristic Grashof number Gr_c and the characteristic Peclet number Pe_c are to be defined for each individual problem. The dimensionless

tensor of the Darcy–Forchheimer drag R_{xx}, R_{xy}, R_{yx}, R_{yy} will be discussed later.

It should be noted that the inertia term in equations (3) and (4) and the heat convection term in equation (5) are based on the superficial velocity of the fluid because the solid is stationary. The second term on the right hand side of the momentum equations represents the viscous force arising from the fluid-to-fluid interaction [7, 8]. It would vanish in a region where the superficial velocity is uniform. However, this particular term could be always considerable in the wall regions where the superficial velocity possesses a sharp variation due to the no-slip condition. In addition, they should govern the drag force alone when the system of governing equations (2)–(5) is directly applied on the pure fluid region by assigning $\varepsilon = 1$. Under such a situation, the Darcy–Forchheimer drag disappears and the system of governing equations becomes that for a single phase problem [7, 8]. Hence, the fluid-to-fluid viscosity term should be simply proportional to the viscosity of the fluid μ as found by Ganesan and Poirier [6] after a rigorous derivation. The widely adopted assumption [5, 9] that the fluid-to-fluid interaction term could have an 'effective' viscosity different from the molecular viscosity μ is not evident.

In the present study, the bank of circular cylinders is modeled as an orthotropic medium. Thus, the tensor of the Darcy–Forchheimer drag R_{xx}, R_{xy}, R_{yx}, R_{yy} appearing in the system of equations (2)–(5) can be evaluated from [10–12]

$$R_{xx} = \frac{1}{2}(R_{11} + R_{22}) + \frac{1}{2}(R_{11} - R_{22})\cos(2\phi)$$

$$R_{xy} = R_{yx} = \frac{1}{2}(R_{11} - R_{22})\sin(2\phi)$$

$$R_{yy} = \frac{1}{2}(R_{11} + R_{22}) - \frac{1}{2}(R_{11} - R_{22})\cos(2\phi) \tag{6}$$

where R_{11} and R_{22} denote the Darcy–Forchheimer drag in the principal axes of the anisotropic porous medium respectively parallel and normal to the cylinders. In this connection, ϕ is the angle between the principal axis 11 and the physical ordinate x.

Recently, Lee and Yang [13] solved the fluid flow across a bank of circular cylinders in pore scale. The velocity then was integrated to yield a modelling for the Darcy–Forchheimer drag in the form

$$R_{22} = \left(\frac{d^2}{K} + F\,Re_{\mathrm{d}}\right)_{22} \tag{7a}$$

$$(Re_d)_{22} = |\bar{U}_{22}|d/v \tag{7b}$$

The Forchheimer drag $(F\,Re_{\mathrm{d}})_{22}$ was found to arise from the form drag on the surfaces of the cylinders. In the present study, this same technique is employed to evaluate the Darcy–Forchheimer drag for fluid flow parallel to a bank of circular cylinders as illustrated in Fig. 1. Due to the particular geometry, only the flow inside a unit cell (with area $l \times l$) is solved on a Cartesian grid system as shown in fig. 2 of ref . [13]. Diameter of the

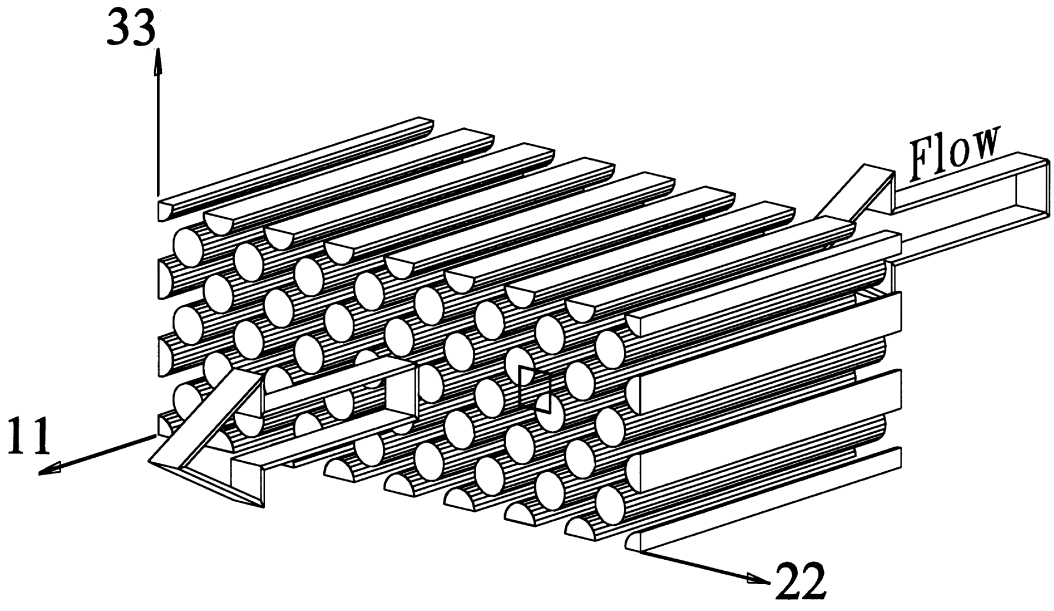

Fig. 1. A schematic sketch for a fluid flow through a bank of circular cylinders.

cylinders d is assigned as the granule size of the porous medium. The resulting Darcy–Forchheimer drag R_{11} is found independent of the granular Reynolds number $(Re_d)_{11}$ due to the absence of the form drag. The correlation

$$R_{11} = \left(\frac{d^2}{K} + F\,Re_d\right)_{11} \tag{8a}$$

$$F_{11} = 0 \tag{8b}$$

$$\frac{d^2}{K_{11}} = -(8.94 - 117.1\varepsilon + 91.26\varepsilon^2)\frac{(1-\varepsilon)^{1.3}}{\varepsilon^3} \tag{9a}$$

$$\varepsilon = 1 - \frac{\pi}{8}\left(\frac{d}{l}\right)^2 \tag{9b}$$

fits the computed R_{11} within a maximum error of less than 5% for all of the possible porosities ($0.2146 \leqslant \varepsilon \leqslant 1$).

Similarly, tensor of the effective thermal conductivity needed in equation (5) is expressible as

$$\kappa_{xx} = \frac{1}{2}(\kappa_{11} + \kappa_{22}) + \frac{1}{2}(\kappa_{11} - \kappa_{22})\cos(2\phi)$$

$$\kappa_{xy} = \kappa_{yx} = \frac{1}{2}(\kappa_{11} - \kappa_{22})\sin(2\phi)$$

$$\kappa_{yy} = \frac{1}{2}(\kappa_{11} + \kappa_{22}) - \frac{1}{2}(\kappa_{11} - \kappa_{22})\cos(2\phi) \tag{10}$$

For a particular porous matrix such as the bank of circular cylinders under study, the principal thermal conductivities κ_{11} and κ_{22} can be effectively determined by a numerical procedure proposed in ref. [14]. For instance, to determine the effective thermal conductivity across the cylinders (κ_{22}), one solves a heat conduction problem in pore scale with a given temperature difference in the principal direction 22. The pore scale temperature as well as the pore scale heat flux then is integrated over cross-sections normal to the principal axis 22. Finally, determine the effective thermal conductivity κ_{22} from the ratio of the averaged heat flux and the gradient of the average temperature. The other principal thermal conductivity κ_{11} can be found similarly. For convenience, the numerical results of κ_{11} and κ_{22} are correlated by

$$\kappa_{11} = \varepsilon + (1-\varepsilon)\sigma = \sigma + (1-\sigma)\varepsilon \tag{11}$$

$$\kappa_{22} = \kappa_{\mathrm{ref}} f(\varepsilon, \sigma)$$

$$\kappa_{\mathrm{ref}} = 1 - \frac{\sqrt{2}}{2}\left(\frac{d}{l}\right) + \sigma\left(\frac{d}{l}\right)\left[(1-\sigma)\frac{d}{l} + \sqrt{2}\sigma\right]^{-1}$$

$$f(\varepsilon, \sigma) = 1 + a(1-\varepsilon)\tan^{-1}(\ln\sigma) + b(1-\varepsilon)^2\tan^{-1}(\ln\sigma) \tag{12}$$

$$\sigma = k_s/k_f$$

$$\frac{d}{l} = \sqrt{8(1-\varepsilon)/\pi}$$

$$a = -0.01373 + 0.1552\tan^{-1}(\ln\sigma - 3.2)$$

$$b = -0.5536 - 0.3913\tan^{-1}(\ln\sigma - 2.5) \tag{13}$$

The correlations (11) and (12) are found to make a good approximation to the computed κ_{11} and κ_{22} with a maximum error of less than 5% for $0.2146 \leqslant \varepsilon \leqslant 1$ and $\sigma \geqslant 1$. In the present study, the granule Peclet number ($Pr\,Re_d$) is not large such that effect of thermal dispersion is neglected [11].

It is interesting to note that for isotropic porous media, the Forchheimer coefficients F_{11}, F_{22}, and F_{33} are determined by the same function of ε and Re_d. In their study, Lee and Yang [13] found that the Forchheimer drag ($F\,Re_d$) in a direction depended on the velocity component in the same direction. This implies that the granule Reynolds numbers for a three-dimensional superficial velocity ($\bar{U}_{11}$, $\bar{U}_{22}$, $\bar{U}_{33}$) should be evaluated from

$$(Re_d)_{11} = |\bar{U}_{11}|d/v \tag{14a}$$

$$(Re_d)_{22} = |\bar{U}_{22}|d/v \tag{14b}$$

$$(Re_d)_{33} = |\bar{U}_{33}|d/v \tag{14c}$$

As a result, the Darcy–Forchheimer drag (R_{11}, R_{22}, R_{33}) could be anisotropic even when the matrix of the porous medium is geometrically isotropic. Such a finding is consistent with Kaviany's suggestion [12]. In many previous investigations (e.g. [5]) the granule Reynolds number for the Forchheimer drag was defined on the basis of $|V|$, i.e.,

$$(Re_d)_{11} = (Re_d)_{22} = (Re_d)_{33} = (\bar{U}_{11}^2 + \bar{U}_{22}^2 + \bar{U}_{33}^2)^{1/2}d/v \tag{15}$$

The assumption of 'isotropic granule Reynolds numbers' obviously ignores the influence of the different velocity components when $\bar{U}_{11} \neq \bar{U}_{22} \neq \bar{U}_{33}$, and thus is questionable in nature.

3. Forced flow through an anisotropic porous medium

Consider an incompressible laminar flow through a channel formed with two parallel flat plates of infinite length. The channel is blocked by a bank of circular cylinders of diameter d. The cylinders are staggered and possess the directional angle (ϕ, $90^\circ - \phi$, 90°) as shown in Fig. 2. Such a directional angle will be referred to as 'an inclination angle ϕ' in the present study for simplicity. Let fluid enter the channel with a uniform temperature T_∞ at $X = -\infty$, while both plates are perfectly insulated except for $T(X, 0) = T_o$ on the heating surface $0 \leqslant X \leqslant W$ and $Y = 0$. Natural convection is assumed negligible. The row spacing of the cylinders (l) is very small as compared to the width of the channel (H) such that the cylinders can be modelled as an anisotropic porous medium. All of the thermophysical properties are constant. Physically, the fluid flow in the present forced

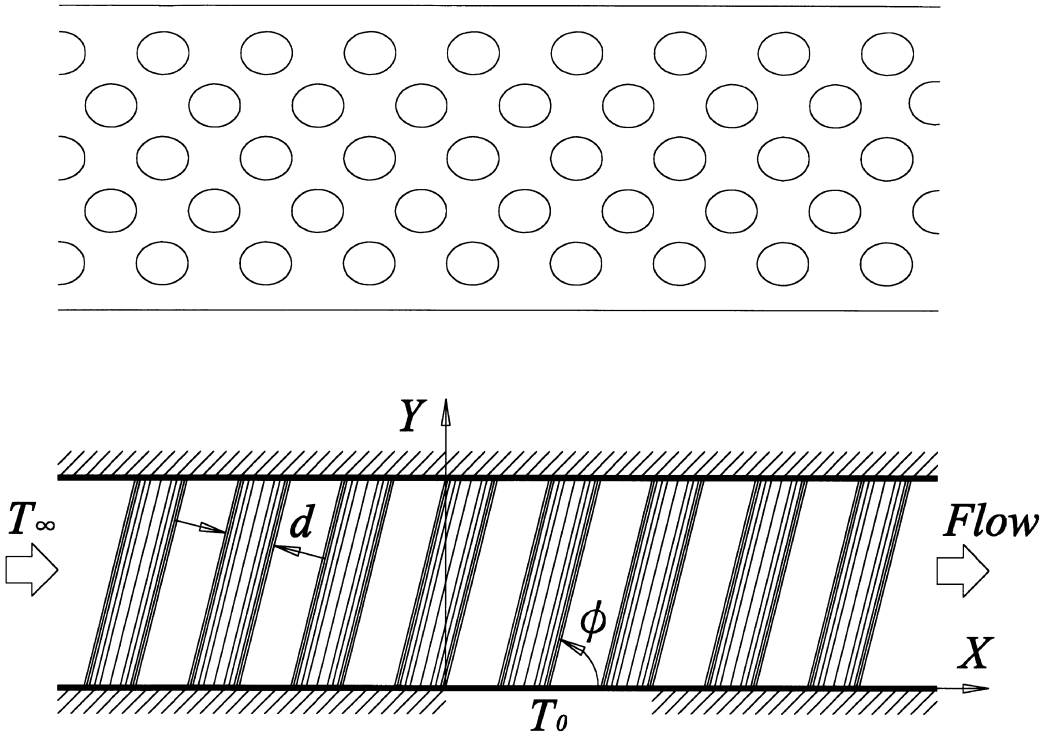

Fig. 2. Top view and front view of the flow configuration in the forced convection example.

convection problem would be momentum fully developed throughout the channel (i.e. $\partial\bar{u}/\partial x = 0$ and thus $\bar{v} = 0$ and $\partial\bar{p}/\partial x$ is constant). Based on these and the following definitions

$$V_c = U_m, \quad L = H, \quad U_m = \dot{m}/(\rho_f H), \quad \Delta T = T_o - T_\infty,$$
$$Re_c = U_m H/\nu = Re, \quad Gr_c = 0, \quad Pr = \nu/\alpha_f,$$
$$Pe_c = Pr\,Re \tag{16}$$

the set of governing equations (3)–(5) reduces to

$$0 = Re\frac{\partial\bar{p}}{\partial x} + \left(\frac{H}{d}\right)^2 R_{xx}\bar{u} - \frac{1}{\varepsilon}\frac{\partial^2\bar{u}}{\partial y^2} \tag{17}$$

$$0 = Re\frac{\partial\bar{p}}{\partial y} + \left(\frac{H}{d}\right)^2 R_{yx}\bar{u} \tag{18}$$

$$Pr\,Re\,\bar{u}\frac{\partial\theta}{\partial x} = \frac{\partial}{\partial x}\left(\kappa_{xx}\frac{\partial\theta}{\partial x}\right) + \frac{\partial}{\partial x}\left(\kappa_{xy}\frac{\partial\theta}{\partial y}\right) + \frac{\partial}{\partial y}\left(\kappa_{yx}\frac{\partial\theta}{\partial x}\right) + \frac{\partial}{\partial y}\left(\kappa_{yy}\frac{\partial\theta}{\partial y}\right) \tag{19}$$

where the Darcy–Forchheimer drag R_{xx} and R_{yx} and the thermal conductivities κ_{xx}, κ_{xy}, κ_{yx} and κ_{yy} should be evaluated from equations (6)–(13) based on the granule Reynolds number

$$(Re_d)_{22} = |\sin\phi\,\bar{u}|Re\left(\frac{d}{H}\right) \tag{20}$$

while the associated boundary conditions are

$$\bar{u}(x,0) = \bar{u}(x,1) = 0 \tag{21}$$

and

$$\theta(-\infty, y) = 0, \quad \partial\theta(\infty, y)/\partial x = 0, \quad \partial\theta(x,1)/\partial y = 0,$$
$$\partial\theta(x,0)/\partial y = 0 \quad \text{for } x < 0 \quad \text{and} \quad x > 1,$$
$$\theta(x,0) = 1 \quad \text{for } 0 \leqslant x \leqslant 1. \tag{22}$$

Next, estimate a value for the pressure gradient ($\partial\bar{p}/\partial x$ = constant) and solve the ordinary differential equation (17) along with the boundary conditions (21) such that the conservation law

$$\int_0^1 \bar{u}\,dy = 1 \tag{23}$$

is satisfied. Once the superficial velocity $\bar{u}$ is known, the pressure distribution $\bar{p}(x, y)$ is determined from equation (18), and the temperature $\theta(x, y)$ is solved from the energy equations (19) and (22) by using the weighting function scheme [15, 16]. Finally, the dimensionless heat transfer rate is evaluated from

$$q = \frac{Q}{k_f\Delta T} = -\kappa_{yy}\int_0^1 \frac{\partial\theta(x,0)}{\partial y}dx \tag{24a}$$

or

$$q = Pr\,Re \int_0^1 \bar{u}(y)\theta(\infty, y)\,dy \tag{24b}$$

In the present example, numerical computations were performed for various inclination angle ϕ and Reynolds numbers Re under the parameters (Pr, σ, ε, H/d, W/H) = (7, 10, 0.6, 20, 1). The discrepancy between the heat transfer rates computed from equation (24a) and (24b) was found less than 0.01%. Numerical results of isobars, superficial velocity $\bar{u}$ and isotherms are depicted in Fig. 3 for $Re = 1$ and $\phi = 0$, 45, 90 and 135° with the increments $\Delta\bar{p} = 5000$ and $\Delta\theta = 0.1$. For convenience, the detailed velocity profile $\bar{u}(y)$ in the wall region ($y \leqslant 0.05$) is provided in Fig. 4 for $\phi = 0$, 30, 60 and 90°.

From the isobars of Fig. 3, one sees that the pressure gradient has a minimum value at $\phi = 0°$ and possesses a maximum at $\phi = 90°$. Due to a stronger Darcy–Forchheimer drag, the velocity profile at $\phi = 90°$ is slightly flatter than that of $\phi = 0°$ as observable from Fig. 4. It is interesting to note from Fig. 3 that for $0 < \phi < 90°$ (say $\phi = 45°$) the pressure has a negative gradient to the lower-right so as to overcome a greater Darcy–Forchheimer drag across the cylinders (R_{22}) while a fully developed flow ($\bar{v} = 0$) is maintained. Similar phenomenon occurs for $90 < \phi < 180°$ because of geometrical symmetry.

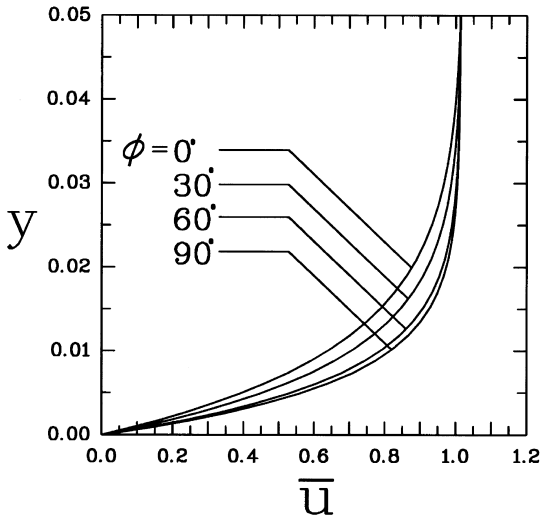

Fig. 4. Velocity profiles in the wall region of the forced flow at $Re = 1$ and $\phi = 0$, 30, 60 and 90°.

In the present computation, the thermal conductivity ratio $\sigma = k_s/k_f$ is as large as 10. The anisotropic thermal conductivity thus could have a great influence on the heat

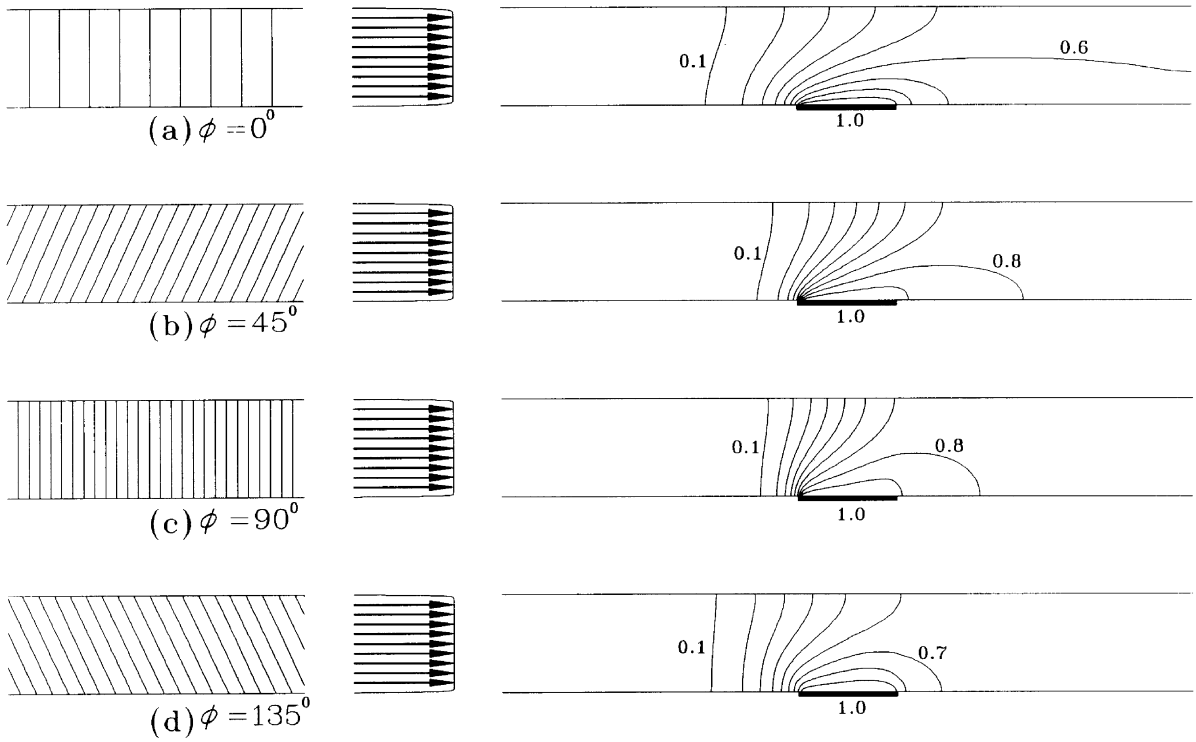

Fig. 3. Isobars ($\Delta\bar{p} = 5000$), superficial velocity $\bar{u}(y)$ and isotherms ($\Delta\theta = 0.1$) for the forced convection at $Re = 1$ and $\phi = 0$, 45, 90 and 135°.

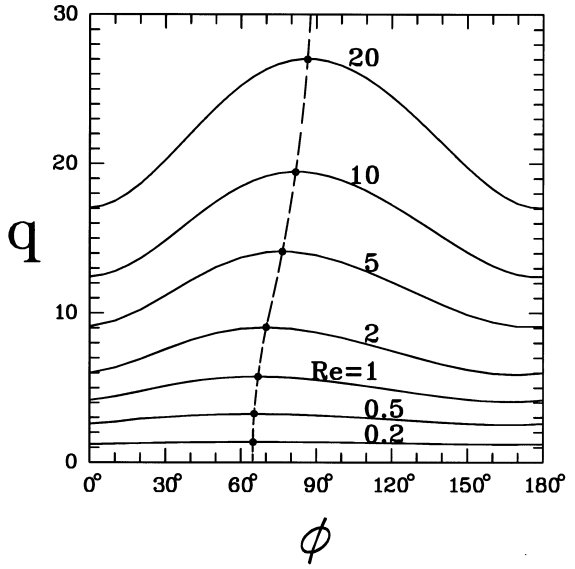

Fig. 5. Heat transfer rate q as a function of ϕ for the forced convection at various Reynolds numbers.

transfer rate q. As observable from Fig. 3(b) and (d), the upstream heat conduction in the case of $\phi = 135^\circ$ is more pronounced than that in the case of $\phi = 45^\circ$, while both cases have the same velocity $\bar{u}(y)$. As a result, the case of $\phi = 135^\circ$ has a lower mean temperature in the downstream region and thus possesses a smaller heat transfer rate q (see equation (24b)).

Figure 5 shows the heat transfer rate q as a function of inclination angle ϕ at various Reynolds numbers under the parameters $(Pr, \sigma, \varepsilon, H/d, W/H) = (7, 10, 0.6, 20, 1)$. The maximum heat transfer rate at each Reynolds number is denoted by the dashed curve. As mentioned in the preceding paragraph, an inclination angle ϕ of less than 90° has a smaller upstream heat conduction and thus a larger heat transfer rate q as compared to the inclination angle $(180^\circ - \phi)$. This might account for the fact that the maximum heat transfer rate occurs at a certain inclination angle below 90°. As expected, the function $q(\phi; Re)$ becomes symmetrical with respect to $\phi = 90^\circ$ when the Reynolds number is sufficiently large such that the forced convection dominates the heat transfer. Nevertheless, the value $(q_{\max}/q_{\min} - 1)$ increases as the Reynolds number increases. It could be even larger than one hundred percent as can be seen from Fig. 5. Therefore, the anisotropy of an anisotropic porous medium could be always very important.

4. Natural convection through an anisotropic porous medium

Consider an anisotropic porous medium inside a square enclosure fully filled with a fluid. Both horizontal walls of the enclosure are insulated while the two vertical walls at $X = 0$ and $X = H$ are maintained respectively at the uniform temperatures T_o and T_∞. The anisotropic porous medium is formed by the same bank of circular cylinders as in the previous example (Fig. 2). After introducing the definitions

$$L = H, \quad V_c = \alpha_f/H, \quad \Delta T = T_o - T_\infty, \quad Pr = \nu/\alpha_f$$

$$Ra = \beta g \Delta T H^3/(\alpha_f \nu) \tag{25}$$

the governing equations are expressible as equations (2)–(5) with the parameters

$$1/Re_c = Pr, \quad Gr_c = Pr\,Ra, \quad Pe_c = 1 \tag{26}$$

The associated boundary conditions are

$$u(0,y) = u(1,y) = u(x,0) = u(x,1) = 0$$
$$v(0,y) = v(1,y) = v(x,0) = v(x,1) = 0$$
$$\theta(0,y) = 1 \quad \theta(1,y) = 0, \quad \partial\theta(x,0)/\partial y = 0$$
$$\partial\theta(x,1)/\partial y = 0 \tag{27}$$

The granule Reynolds number $(Re_d)_{22}$ dealing with the principal Darcy–Forchheimer drag R_{22} should be evaluated from

$$(Re_d)_{22} = |\bar{U}_{22}|d/\nu = |\sin\phi\,\bar{u} - \cos\phi\,\bar{v}|\frac{1}{Pr}\frac{d}{H} \tag{28}$$

The principal Darcy drag R_{11} and the principal effective thermal conductivities k_{11} and k_{22} are the same as that of the forced flow illustrated in the previous section.

Numerical results including the superficial velocity, the pressure and the temperature were obtained for the parameters $(Ra, Pr, \sigma, \varepsilon, H/d) = (10^7, 7, 10, 0.6, 40)$ at various inclination angles ϕ. Upon knowing the superficial velocity and the temperature, the stream function was computed from

$$\psi = \int_0^y \bar{u}\,dy \tag{29a}$$

and

$$\psi = -\int_0^x \bar{v}\,dx \tag{29b}$$

while the heat transfer rate was evaluated from

$$q = \frac{Q}{k_f \Delta T} = -\kappa_{xx}\int_0^1 \frac{\partial\theta(0,y)}{\partial x}\,dy \tag{30}$$

All of the computations were performed on a Cartesian grid system with $\Delta x = \Delta y = 0.02$ by using the weighting function scheme [15, 16] and the NAPPLE algorithm [17]. A further reduction on the grid size did not show significant influence on the numerical solution. In addition, the resulting stream function based on equation (29a) was found to agree with that from equation (29b) at a maximum discrepancy of less than 0.01%. This is a proof on the correctness of the present computations.

Numerical results of isotherms and streamlines are presented in Fig. 6 for the four representative inclination

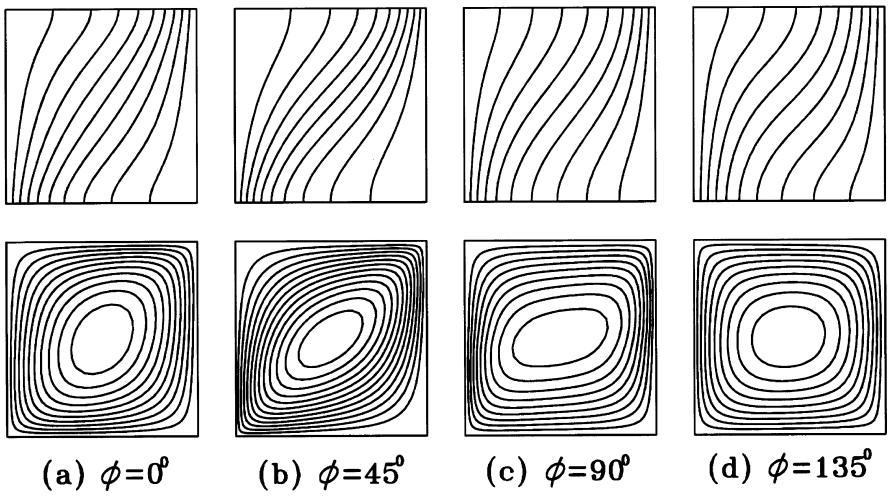

Fig. 6. Isotherms and streamlines ($\Delta\theta = 0.1$ and $\Delta\psi = 0.5$) for the natural convection with $\phi = 0$, 45, 90 and 135°.

angles $\phi = 0$, 45, 90 and 135°. For each of the four cases, the isotherms vary from $\theta = 1$ on the left wall ($x = 0$) to $\theta = 0$ on the right wall ($x = 1$) with an increment of $\Delta\theta = 0.1$. Similarly, the streamlines decrease from $\psi = 0$ on the sold walls toward the center of the square enclosure with an increment of $\Delta\psi = 0.5$. This implies the existence of a minimum stream function $\psi = \psi_{\min} < 0$. Note that negative stream function means a clockwise vortex. Thus, the value of $-\psi_{\min}$ makes a good measure for the strength of a natural convection. For convenience, the value of $-\psi_{\min}$ along with the heat transfer rate (q) is shown in Fig. 7 as functions of ϕ. The heat transfer rate under pure heat conduction situation ($Ra = 0$) also is provided in Fig. 7 as a reference.

It is well-known that in a conventional natural convection inside a square enclosure (without an anisotropic porous medium) the streamlines are slightly elliptic with the long axis lying in the direction of 45° due to the growth of the boundary layers along both vertical walls. The strongest circulating flow in the present problem thus occurs at this particular inclination angle of $\phi = 45°$ due to the smallest Darcy–Forchheimer drag, see Figs 6(b) and 7. Note also that large Darcy–Forchheimer drag near the horizontal walls ($y = 0$ and $y = 1$) could significantly retard the flow because there is no driven force. In the range of inclination angles $90 < \phi < 180°$, the Darcy–Forchheimer drag on both horizontal walls thickens the boundary layer and thus weakens the circulation flow as observable from Figs 6(c), 6(d) and 7.

Again, the thermal conductivity ratio σ in this example is as large as 10. Under such a situation, the horizontal cylinders in the case of $\phi = 0°$ (also 180°) make good 'bridges' for the heat flow from the hot wall to the cold wall. In contrast, the heat flow in the case of $\phi = 90°$ should go across the fluid region that possesses a low

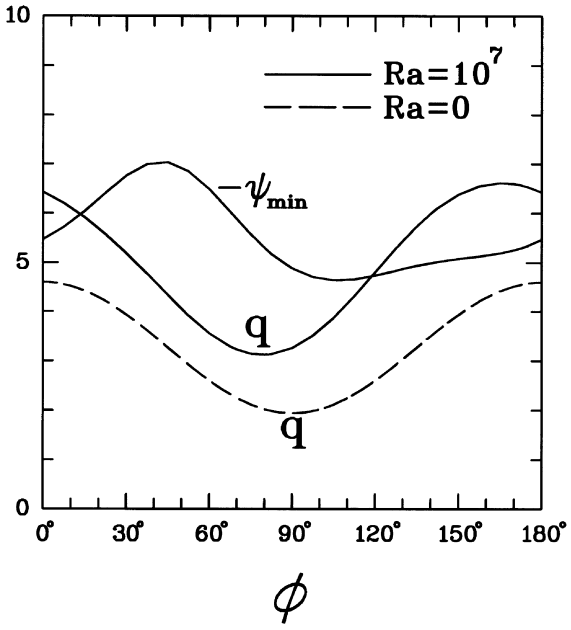

Fig. 7. Strength ($-\psi_{\min}$) and heat transfer rate (q) of the natural convection at various inclination angles.

conductivity. Hence, the best and the worst heat transfer rates occur respectively at an inclination angle near $\phi = 165°$ and $\phi = 80°$ (see Fig. 7). It is interesting to note from Fig. 6 that due to its elliptic streamlines the inclination angle of $\phi = 45°$ has a smaller temperature gradient ($-\partial\theta/\partial x$) on the vertical walls than does the inclination angle $\phi = 135°$. As a result, the heat transfer rate at $\phi = 45°$ is smaller than that at $\phi = 135°$ (see Fig.

7), although both cases have the same effective thermal conductivity κ_{xx}. As a final note, it is mentioned that the heat transfer rate as shown in Fig. 7 can be found to have a variation ($q_{max}/q_{min}-1$) of more than 100%. This implies that the anisotropy of an anisotropic porous media should not be ignored.

5. Conclusion

A bank of circular cylinders is treated as an anisotropic porous medium to investigate the effect of anisotropy on fluid flow and heat transfer in anisotropic porous media. The Darcy–Forchheimer drag and the effective thermal conductivity in the principal axes are determined numerically by using the weighting function scheme along with the NAPPLE algorithm. Modelling of the Darcy drag and the effective thermal conductivity then is derived from the numerical results. Based on the modelling, fluid flow and heat transfer for a forced flow as well as a natural convection through a bank of circular cylinders are solved.

The solutions show that in the forced flow case an inclination of acute angle ϕ has a smaller upstream heat conduction and thus a larger heat transfer rate q as compared to the inclination angle $(180^\circ-\phi)$. As expected, the function $q(\phi)$ becomes symmetrical with respect to $\phi = 90^\circ$ when the Reynolds number is sufficiently large such that the forced convection dominates the heat transfer. Nevertheless, an increase in the Reynolds number enhances the variation on the function $q(\phi)$.

In the natural convection case, the strongest circulating flow occurs at the particular inclination angle of $\phi = 45^\circ$ due to the smallest Darcy–Forchheimer drag. The horizontal cylinders in the case of $\phi = 0^\circ$ (also 180°) make good 'bridge' for the heat flow from the hot wall to the cold wall, and thus have a good heat transfer rate. The solutions reveal also that due to a strong circulation flow the inclination angle of $\phi = 45^\circ$ gives rise to a small temperature gradient $(-\partial\theta/\partial x)$ on the vertical walls and thus poses a small heat transfer rate. The inclination angle is found to have an influence of more than one hundred percent on the heat transfer rate. Hence, the anisotropy of an anisotropic porous medium could be always very important for either forced flow or natural convection.

Acknowledgement

The authors wish to express their appreciation to the National Science Council of Taiwan for the financial support of this work through the project NSC86-2212-E007-066.

References

[1] S. Torquato, Random heterogeneous media: microstructure and improved bounds on effective properties, Applied Mechanics Review 44 (1991) 37–76.
[2] D.R. Poirier, Permeability for flow of interdendritic liquid in columnar-dendritic alloys, Metallurgical Transaction 18B (1987) 245–255.
[3] S.K. Sinha, T. Sundararajan, V.K. Garg, A variable property analysis of alloy solidification using the anisotropic porous medium approach, International Journal of Heat and Mass Transfer 35 (1992) 2865–2877.
[4] H. Yoo, R. Viskanta, Effect of anisotropic permeability on the transport process during solidification of a binary mixture, International Journal of Heat and Mass Transfer 35 (1992) 2335–2346.
[5] C. Beckermann, R. Viskanta, Double-diffusive convection during dendritic solidification of a binary mixture, PhysicoChemical Hydrodynamics 10 (1988) 195–213.
[6] S. Ganesan, D.R. Poirier, Conservation of mass and momentum for the flow of interdendritic liquid during solidification, Metallurgical Transaction 21B (1990) 173–181.
[7] H.C. Brinkman, A calculation of the viscous force exerted by a flowing fluid on a dense swarm of particles, Applied Scientific Research A1 (1947) 27–34.
[8] B.K.C. Chan, C.M. Ivey, J.M. Barry, Natural convection in enclosed porous media with rectangular boundaries, ASME Journal of Heat Transfer 92 (1970) 21–27.
[9] P. Cheng, Heat transfer in geothermal systems, in: T.F. Irvine, Jr., J.P. Hartnett (Eds.), Advances in Heat Transfer, vol. 14., Academic Press, New York, 1978, p. 6.
[10] A.E. Scheidegger, The Physics of Flow Through Porous Media, 3rd ed., University of Toronto Press, Toronto, 1974.
[11] F.A.L., Dullien, Porous Media: Fluid Transport and Pore Structure, 2nd edn., Academic Press, San Diego, 1992, Ch. 6, pp. 303–306.
[12] M. Kaviany, Principles of Heat Transfer in Porous Media, 2nd ed., Springer-Verlag, New York, 1995, pp. 19–20, 47–48.
[13] S.L. Lee, J.H. Yang, Modeling of Darcy–Forchheimer drag for fluid flow across a bank of circular cylinders, International Journal of Heat and Mass transfer 40 (1997) 3149–3155.
[14] S.L. Lee, J.H. Yang, Modelling of effective thermal conductivity for a nonhomogeneous anisotropic porous medium, International Journal of Heat and Mass Transfer 41 (1998) 931–937.
[15] S.L. Lee, Weighting function scheme and its application on multidimensional conservation equations, International Journal of Heat and Mass Transfer 32 (1989) 2065–2073.
[16] K. Hsu, S.L. Lee, A numerical technique for two-dimensional grid generation with grid control at all of the boundaries, Journal of Computational Physics 96 (1991) 451–469.
[17] S.L. Lee, R.Y. Tzong, Artificial pressure for pressure-linked equation, International Journal of Heat and Mass Transfer 35 (1992) 2705–2716.